# Water in Ice — It's Detection, Measurement and Role in Understanding Glacial Acceleration and Melt Processes from ICESat-2 Altimeter Data

**Ute Herzfeld[1],Rachel Middleton[1,2],Thomas Trantow[1], and Adam Hayes[1]**

[1]Geomathematics, Remote Sensing and Cryospheric Sciences Laboratory, Department of Electrical, Computer and Energy Engineering, University of Colorado Boulder, Boulder, CO, USA
[2]Department of Civil,Environmental and Architectural Engineering, University of Colorado, Boulder, CO, USA

**Key Points:**

- Supraglacial water features are recorded by NASA's ICESat-2 and identified with higher order DDA-ice algorithms
- Water in crevasses is an indicator of switches in the dynamic state of a surge glacier, and these switches are not detectible otherwise
- Water in melt ponds and streams on glaciers and ice sheets provides an essential indicator of melt progression in a warming climate

Corresponding author: Ute Herzfeld, `ute.herzfeld@colorado.edu`

## Abstract

While melt-driven occurrence of supraglacial water is largely recognized, an essential but overlooked component of supraglacial water appearance is glacial dynamics and their interaction with hydrological drainage systems. ICESat-2 ATLAS data record returns from water features, which requires an automated method for detection and depth measurement. We introduce second-order Density-Dimension (DDA-ice) algorithms that facilitate detection of water in crevasses and melt features. Density characteristics from the DDA-ice allow identification of cryospheric material types such as snow, water-logged firn and water in crevasses. Application of the DDA-ice-2 to data from the current surge of Negribreen, Svalbard, yields key informants on englacial hydrological changes that control the surge process, but are hard to detect otherwise. Analysis of melt ponds and streams on the Greenland Ice Sheet and the Amery Ice Shelf illustrate the capability of the DDA-bifurcate to extract complex morphological shapes, a characteristic that suggests application in morphogenesis of glacio-hydrological features.

## Plain Language Summary

It is well-known that increasing climatic warming is leading to increased melting of the Earth's glaciers and ice sheets, as is indicated by increased occurrence of melt ponds and melt streams on the ice. An additional but overlooked component of supraglacial water appearance is glacial dynamics and their interaction with hydrological drainage systems. Rapid observable changes in ice dynamics are the characteristics of glacial surges, which are accelerations of a glacier to 10-200 or more times their normal flow velocity. To better understand the mechanisms through which water affects movement and mass loss, this work establishes a new approach for measurement of water on, and implicitly, in, ice, using ICESat-2 ATLAS high-resolution satellite laser altimetry data. To this end, we introduce higher-order Density-Dimension Algorithms for ice surfaces (DDA-ice), which are applied to detect and measure the depth of several kinds of water features: (1) Water in crevasses during the current surge of an Arctic Glacier provides information on the glacial dynamics of this catastrophic process. (2) Water in melt streams of Amery Ice Shelf indicates a rare melt event in Antarctica, and application to data from the Greenland Ice Sheet allows understanding of complex melt processes.

## 1 Water In and On Ice as a Signature of Glacial Acceleration and Melt Processes

Increased occurrence of water on ice has seen attention in the cryospheric community and beyond as an alarming sign of the impeding loss of glaciers, ice sheets and Arctic sea ice in the current realm of climatic warming (Markus et al., 2009; Schoof, 2010; Nghiem et al., 2012; Bartholomew et al., 2012; Hall et al., 2013; Fricker et al., 2020; Spergel et al., 2021; Buckley et al., 2023; U. Herzfeld et al., 2023). In addition to melting, water on glaciers and ice streams can also occur as a result of changes in ice dynamics (Fig. 1).

Rapid observable changes in ice dynamics are the characteristics of glacial surges, which are accelerations of a glacier to 10-200 or more times their normal flow velocity. Glacial acceleration is one of two major sources of uncertainty in SLR assessment, a problem identified by the Intergovernmental Panel on Climate Change (IPCC) Assessment Report (AR) 5 (Stocker et al., 2013). The AR 6 (Masson-Delmotte et al., 2021) used the term "deep uncertainty" to emphasize the importance of this still unsolved problem and its relationship to ice-dynamical instabilities. Surging is a type of glacial acceleration (Clarke, 1987; Truffer & Echelmeyer, 2003), and is the least understood type because surges are relatively rare events and thus comprehensive observations are limited relative to other acceleration types. While valuable dedicated surge studies exist, e.g. (Mayer & Herzfeld, 2000; U. Herzfeld et al., 2013; Kochtitzky et al., 2020; Banerjee et al., 2022; Liu et al., 2024; Main et al., 2024; Trantow & Herzfeld, 2024a, 2024b), our community's ability to analyze the surge process is limited. Mass loss from a single Arctic glacier during surge can equate to 0.5-1% of annual global sea-level rise (SLR) in only a few months, as was observed during the height of the current surge of Negribreen, Svalbard (Fig. 1m), in summer 2017 (U. Herzfeld, Trantow, et al., 2021; U. C. Herzfeld et al., 2022), a finding that highlights the importance of surges in SLR. The first focus of this paper will be the detection of water in crevasses during the surge of the Negribreen Glacier System (NGS) and interpretation of its role.

The acceleration phase of the surge is characterized by opening of crevasses. As the surge progresses, suddenly water-filled crevasses will occur locally and later on more pervasively throughout the surging glacier (Fig. 1e-h). These water-filled crevasses result from the transition of the englacial glaciological system from an efficient drainage system (EDS) to an inefficient drainage system (IDS) resultant from the destruction of existing drainage path caused by the rapid motion of the glacier during surge (Kamb, 1987), a process that can be spatiotemporally complex as analyzed in numerical modeling studies (Trantow & Herzfeld, 2018, 2024a). Thus surface water is a signature of otherwise hard-to-observe changes in the interior of the glacier which control the unique dynamics of a surge and the hitherto incompletely understood evolution of hydrological changes. This signature characteristic, combined with investigation of supraglacial and near-surface water, motivates the terminology "water in ice" as the focus of this study. An objective of this paper is to demonstrate that satellite laser altimeter data from NASA's ICESat-2 Mission (Markus et al., 2017; T. A. Neumann et al., 2019) can be utilized to extract information on water in crevasses. We will introduce a mathematical approach that facilitates detection of water in crevasses and measurement of its depth, based on the Density-Dimension Algorithm for ice surfaces (DDA-ice) (U. Herzfeld, Trantow, et al., 2021). Furthermore, the work in this paper will shed some light on the characterization of different cryospheric materials, such as snow and water-logged firn that occur in crevasses during various stages of the melt process, as afforded by a generalization of the DDA-ice.

The second focus of the paper will return to the problem of observation and measurement of melt features on glaciers, ice shelves and ice sheets. Recent studies have investigated the geophysical processes responsible for the increased melt of the Greenland Ice Sheet (Tedesco et al., 2016; Stroeve et al., 2017; Wood et al., 2018; Oltmanns et al., 2019; Ryan et al., 2019). It has long been known that the coupling between surface meltwater and ice flow can lead to rapid and large-scale dynamic changes in the ice sheets and glaciers (Zwally et al., 2002; McMillan et al., 2007). Satellite image technology has allowed observations of supraglacial lakes on the Greenland Ice Sheet (Sneed & Hamilton, 2007; Sundal et al., 2009; Moussavi et al., 2016; Williamson et al., 2018). (Fricker et al., 2020) compare derivation of melt-stream depth from image data during a melt event on the Amery Ice Shelf, Antarctica, with approaches for retrieval of melt-stream depth from ICESat-2 ATLAS data, a technology further developed in (Arndt & Fricker, 2024). Common to the cited approaches is that melt-pond location in ICESat-2 data requires a-priori information and determination of the second surface, the bottom of the melt feature, is only attainable for large (several hundred meter diameter) water bodies with well-defined secondary returns in the ICESat-2 ATL03 data. To remedy this situation, we will briefly describe melt-feature determination in ICESat-2 data using an algorithm of the DDA family, the DDA-bifurcate (U. Herzfeld et al., 2023), which allows detection and depth measurement of shallow, small and complex melt features, thus facilitating a more detailed basis for the study of melt processes in glaciers and ice sheets. The DDA-bifurcate builds on the DDA-bifurcate-seaice (U. Herzfeld et al., 2023) which has been applied to detect ponds down to 7.5 m in diameter and 0.1 m in depth.

## 2 ICESat-2 ATLAS Data as a Source of Information on Water in Ice

NASA's Ice, Cloud and land Elevation Satellite, ICESat-2, launched September 15, 2018, was designed to map high-resolution changes in the surface elevation of glaciers, ice sheets and sea ice, as well as collect information on vegetation cover and atmospheric layers (Markus et al., 2017; T. A. Neumann et al., 2019). With the Advanced Topographic Laser Altimeter System (ATLAS), ICESat-2 carries the first space-borne multi-beam micro-pulse photon-counting laser altimeter system. While ATLAS was not expected to measure more than the primary surface of the Earth for glaciers, ice sheets, ice shelves and sea ice, the recorded photon point cloud, reported on ICESat-2 ATLAS data product ATL03 (T. Neumann et al., 2022b), captures returns from secondary surfaces, such as bottom reflectors of melt ponds over land ice and sea ice (Farrell et al., 2020; U. Herzfeld et al., 2023; Fricker et al., 2020). Extraction of this information requires development of a new algorithmic approach.

With ATLAS, ICESat-2 operates a 532 nm, green-light, micro-pules photon-counting lidar altimeter at 10KHz pulse-repetition frequency, which results in a nominal along-track spacing of 0.7 m (under clear-sky atmospheric conditions). ATLAS has three sets of two beams (a weak beam and a strong beam, where the energy of the weak beam is 1/4th that of the strong beam). The geometry of the beam pattern and the dependence of numbering of beams and spots on orientation of the observatory is described in Fig. 3 and Table 1 of (U. Herzfeld, Trantow, et al., 2021). All DDA-ice algorithms take ATL03 geolocated photon data (T. Neumann et al., 2022a) as input.

## 3 Mathematical Methods: Detection of Crevasses, Water in Crevasses and Water in Melt Features using the Density Dimension Family of Algorithms

### 3.1 Overview of Density Dimension Algorithms for Ice Surfaces

Detection of crevasses, both dry and water-filled, and detection of melt features on the ice surface is accomplished by application of the Density-Dimension Family of Algorithms. The density-dimension algorithms are a suite of algorithms specifically developed for the analysis of ICESat-2 ATLAS data and more generally, micro-pulse photon-counting lidar altimeter data. The analysis in this paper utilizes the following algorithms: (1) The Density-Dimension Algorithm (DDA) for ice surfaces (DDA-ice, or DDA-ice-1) has been developed for surface height determination of crevassed and otherwise morphologically complex ice surfaces and also works for smooth ice surfaces (U. Herzfeld et al., 2017; U. Herzfeld, Trantow, et al., 2021). (2) Detection of secondary surfaces, defined here as surfaces of lower backscatter intensity than those of primary surfaces, is possible with the DDA-ice-2. The DDA-ice-2 is a second-order algorithm that builds on the DDA-ice-1. Here, the DDA-ice-2 is employed for detection of water in crevasses, including reflectors that stem from snow or firn transforming into water. (3) Detection of melt streams and ponds requires the application of the DDA-bifurcate, whose name indicates the detection and height determination of bifurcating surfaces (melt-pond top and melt-pond bottom). The DDA-bifurcate is a two-level algorithm; its development has been necessitated by the fact that, for melt ponds, the stronger reflecting surface can be either the bottom or the top.

Other members of the DDA algorithm family include the DDA-atmos, which is used as the official algorithm for ICESat-2 atmospheric products (cloud and aerosol layers, blowing snow and diamond dust)(U. Herzfeld, Hayes, et al., 2021; U. Herzfeld et al., 2022). The DDA-ice has been validated for surface-height determination of an Arctic surge glacier during surge (U. C. Herzfeld et al., 2022) and applied to two years of ICESat-2 data to derive glaciological processes during the surge (Trantow & Herzfeld, 2024b).

### 3.2 Mathematical Principles of the DDA-ice

All DDA methods are built around the calculation of the density field and a density-based separation between signal and background ("noise") that, motivated by the notion that a geophysically valid reflector (such as the ice surface or the bottom of a melt pond) has a higher density of photons in the received point cloud than background. The radial basis function is the basic mathematical concept used in the data aggregation for calculation of density. The data aggregation by density calculation forms the basis for all other steps of the DDA (U. Herzfeld et al., 2017; U. Herzfeld, Trantow, et al., 2021), which include threshold separation of signal and background photons and application-specific ground followers. The DDA-ice-1 for ATLAS data utilizes the geolocated photon cloud as reported in the ATLAS product ATL03 (but not the photon classification given in ATL03). Data postings of the density field have the same spatial resolution as the original data, and surface heights are reported at near-sensor resolution, for example, at 2.5 m along-track for crevassed surfaces and 5 m along-track for smooth surfaces.

A *radial basis function (rbf)* is a real-valued function whose value depends on distance from a *center* $c \in \mathcal{D}$ for all $x$ in a definition area $\mathcal{D}$

$$\Phi(x, c) = \Phi(\|x - c\|) \tag{1}$$

with respect to any norm $\|\cdot\|$. In the algorithm, a Gaussian radial basis function is used (letting $r = x - c$ and $s \in \mathcal{R}$)

$$\Phi(r) = e^{-(\frac{r}{\sqrt{2}s})^2} \tag{2}$$

Visualized as a surface in $\mathcal{R}^3$, this *rbf* kernel has the shape of (half) a Gaussian bell curve rotated around the location of a center $c \in \mathcal{R}^2$. In the photon-data analysis, $c \in \mathcal{R}^3$ and the surface is in $\mathcal{R}^4$. More formally, the Gaussian probability density function is

$$f_{normpdf} = \frac{1}{\sqrt{2\pi\sigma^2}} e^{-(\frac{x-\mu}{\sqrt{2}\sigma})^2} \tag{3}$$

with standard deviation $\sigma$ and mean $\mu$ of the population; replacing $\sigma = s$ and $\mu = 0$ yieldfs eqn. (4):

$$\Phi(r) = \sigma\sqrt{2\pi} f_{normpdf} \tag{4}$$

Following the calculation of the density field, an auto-adaptative threshold function is applied to separate signal and background photons. The auto-adaptive capability means that the algorithm adapts automatically to changes in background in the photon point cloud, as are typical for night-time data (low background) and day-time data (high background) and changes in apparent surface reflectance, which may be caused by changes in albedo of the ice surface. In addition, the auto-adaptive threshold function can correct for some undesired instrument effects.

The DDA-ice is an auto-adaptive algorithm, which uses the mathematical concept of an artificial neural network (NN) (the *rbf*) in an entirely new way, but it is not a NN. Herein lies the reason that, while conceptually advanced, the DDA is computationally inexpensive, a property which makes it feasible to process surface heights for the entire cryosphere.

The DDA-ice utilizes a ground-following algorithm that adapts to the roughness of the surface or the crevasse morphology, with higher resolution for rough surfaces, such as crevassed ice surfaces, and lower resolution for smooth surfaces. All DDA algorithms are driven by a set of algorithm-specific parameters, which can be optimized, but once the parameters are set, the algorithm will run without further adjustment ("auto-adaptively"). Before running the actual DDA-ice, a cloud-ground separation algorithm is applied to ascertain that returns from clouds are not mistaken for ground returns. The algorithm steps are illustrated in ((U. Herzfeld, Trantow, et al., 2021), Fig. 4, see also Fig. S1) with parameters given in Table S1.

### 3.3 Detection of Water in Crevasses: DDA-ice-2

The DDA-ice-1 performs the following steps, (0) cloud-ground separation, (1) signal-noise separation, (2) calculation of the density field, (3) auto-adaptive threshold function, (4) surface-height determination (using a roughness-adapting ground follower). The main idea for detection of a secondary surface is to analyze the data field of the photons that remain after the photons identified as primary signal returns are masked out. This is accomplished by a trick termed "running density twice": We run algorithm steps (0) through (4), which results in the signal photons heights from density-1. Then the steps (2)-(4) are applied to the field of remaining photons, but with different parameters, optimized to capture the characteristics of a second-order reflector. For example, a large kernel is used in density-run two to find a weak reflector. For the problem of water-in-crevasses, a similar type of ground follower is used for the second surface as for the primary surface. The maximal depth of water in crevasses can be estimated from the difference of the two surfaces at the bottom of a crevasse.

### 3.4 Depth Measurement of Water in Crevasses

To derive an estimate of depth of water in crevasses, we use a simple ad-hoc approach in this paper, based on the apparent water depth in the two photon surface height profiles, which is calculated from range, and correction for the speed of light in water. For each crevasse, we determine apparent water depth as the difference between the lowest point in the top surface profile (water surface) and the lowest point in the bottom surface profile (crevasse bottom), identified by the surface followers of the DDA-ice-2.

The true depth of water is then determined by correcting for the speed of light in water, according to Snell's Law:

$$d_{true} = \frac{d_{app}}{n_{water}} \tag{5}$$

Where $d_{true}$ is the actual depth of water in the crevasse, $d_{app}$ is the apparent depth of water or the range difference, and $n_{water}$ is the refractive index of light in water, 1.33.

In figure 1d, the apparent depth of the water-filled crevasse is approximately 7.0 m. When corrected for the speed of light in water, the real depth is 5.4 m.

### 3.5 Detection and depth measurement of water in melt ponds: DDA-bifurcate

The idea of a bifurcating algorithm is to identify locations where two geophysically valid surfaces exist (U. Herzfeld et al., 2023). The DDA-bifurcate aims to accomplish this for analysis of the ICESat-2 ATL03 photon cloud over land ice surfaces. A key feature of the DDA-bifurcate is the ability to detect bifurcating reflectors in situations where the stronger reflector can be the lower or the higher reflector and the two reflectors may have different spatial distributions and material/reflection properties. The algorithm applied here to the detection of melt ponds and melt streams on ice sheets and ice shelves is similar to the DDA-bifurcate-seaice (DDA-bif-seaice for short), developed for the problem of melt ponds on Arctic sea ice, described in (U. Herzfeld et al., 2023). Because sea-ice melt ponds are much smaller and more shallow than land-ice water features, the problem of their detection and depth measurement is mathematically more difficult.

## 4 Results I: Detection of Water in Surge Crevasses as Indicator of Mature Surge Phase Processes

[FIGURE 1 here]

### 4.1 Crevassing and Detection of Crevasses in ICESat-2 ATLAS Data

The objective of this section is to demonstrate applications of analyses of dry and wet crevasses as indicators of surge evolution for the current surge of the NGS. The DDA-ice-1 facilitates surface-height determination of crevassed ice surfaces in ICESat-2 ATLAS, as described in (U. Herzfeld, Trantow, et al., 2021; U. C. Herzfeld et al., 2022). This detection capability, which has been applied to analyze the surge process in the NGS based on two years of ICESat-2 data (2019 and 2020) (Trantow & Herzfeld, 2024b), is illustrated in Figures 1a,b,j. At first impression, the results in these three figures are similar.

In addition to crevasses as morphological features, the ICESat-2 photon point cloud includes information on occurrence of water in crevasses, as is typical during the mature phase of a surge. As a first approximation, this can be derived from the density field, calculated by the DDA-ice-1. Comparison with co-located airborne image data, collected during our ICESat-2 airborne validation campaign over the NGS within several days of the ICESat-2 data acquisition (U. C. Herzfeld et al., 2022), shows that the segment in Fig. 1a (from ICESat-2 Reference Ground Track (RGT) 450) stems from an area with dry crevasses which are partly filled with old snow (Fig. 1e,f), whereas the segment in Fig. 1b,j (from RGT594) stems from an area of wet crevasses and crevasses with firn close to melting (Fig. 1g,h). As both the GoPro image (Fig. 1e) and the density field for RGT450 indicate, there are a few exceptions, which consist of areas of old snow just starting to melt. Closer scrutiny of the density fields indicates that clusters of photons with relatively high density are associated with the wet-crevasse area. The density value associated with a photon is indicated by the color of the larger, colored dots (for a photon identified as signal), with background photons given as small, black dots. Areas of waterlogged, dense firn are depicted as green clusters (Figs. 1b,j), whereas areas of dry/less dense snow appear as blue signal photon clusters (Fig. 1a). Standing water appears as a horizontal segment of photons, returned from the surface of the water body in a crevasse (Fig. 1b,d) [note that the RGT594 crosses the edge of the field of wet crevasses, Fig. 1i]. The next algorithmic objective is the identification of a secondary surface related to water detection: The DDA-ice-2 (section (4.2)).

### 4.2 Occurrence of Water in Crevasses and its Detection and Measurement in ICESat-2 Data. Density as an Indicator of Cryospheric Materials

As the surge progresses, a new phase is entered, called the mature phase of the surge. Characteristic of this phase is the sudden occurrence of water locally in some crevasse fields. Detection of water in crevasses, which is the signature of a change in the englacial hydrological system of the glacier, requires a new algorithm capability. This is where the DDA-ice-2 comes in.

Application of the DDA-ice-2 to the data from RGT594 results in the identification of a secondary surface that follows the bottoms of the water-filled crevasses. Figs. 1d,k demonstrate that the areas of higher density, indicative of water-logged firn identified in Figs. 1b,j (section (4.1)), are located between the upper (red line) and the lower (green line) surface heights (see also Supplement Fig. S1). In Figure 1d, the apparent depth of the water-filled crevasse is approximately 7.0 m, using the approach described in (3.4). When corrected for the speed of light in water, the true depth is 5.3 m.

Cross-reference between ICESat-2 data and satellite image data, given in Figures 1i, l, serves two purposes. First, the location of the two reference ground tracks (RGTs), superimposed on a MAXAR WorldView-1 image, indicates that the three examples stem from crevasse fields in the region in upper Negribreen, which opened at a similar time (in 2017, per our field observations (U. C. Herzfeld & Trantow, 2021)). One of these crevasse fields transformed into an area of wet crevassing, indicating the localized nature of wet versus dry crevassing.

Segment 12 of RGT594 crosses the edge of a field of wet crevasses, allowing identification of a single crevasse with standing water, whereas adjacent crevasses in segments 12 and 13 contain water-logged firn that is close to melting, and this situation can be identified using the DDA-ice-2. In contrast, segment 24 of RGT 450 crosses a field of crevasses filled with old snow. Because there is typically a lack of coincident data between different types of satellites (ICESat-2, LandSat) and airborne observations, we extend the analysis of water in crevasses to water-logged firn in crevasses, as a means to form a larger data base across larger time differences of observations during which the snow can melt. In our analysis, the satellite image for the NGS is from 2019-08-11, field data from 2019-08-13, RGT594 data from 2019-08-05 and RGT450 data from 2019-07-29. The combination of satellite imagery, imagery from the airborne validation campaign and analysis with the DDA-ice-1 and the DDA-ice-2 facilitates the identification of different cryospheric materials inside the crevasses (water, water-logged firn, old snow) which cannot be achieved from imagery alone. In conclusion, the DDA-ice-2 approach yields localized information on the transition between dry and wet crevassing and thus provides a unique type of additional information, which cannot be derived from image analysis.

Furthermore, the analysis suggests that a proxy classification of cryospheric materials based on the density value may be feasible. The DDA-ice-2 identifies the crevasse bottom as a secondary surface also for the field of crevasses filled with old snow (Fig. 1c), because of the density difference between the primary reflector (here: old snow that has fallen into the crevasses) and the secondary reflector (crevasse bottom). In all cases of crevasses that are partly filled with a different material than ice, we derive the height difference of surface-from-density-1-run minus surface-from-density-2-run. Then, density characteristics can be used to identify wetness of the material in the crevasses. More specifically, these density characteristics are based on relative density of clusters of signal photons (for more detailed information on the material characterization, see Supplement, section 1). Regardless of the material that may be obstructing the laser's view of the crevasse bottom, the DDA-ice-2 always finds the surface height of the crevasse bottom (see also, (U. C. Herzfeld et al., 2022)).

## 5 Results II: Melt Features

Melt pond occurrence, depth, and morphology are extracted from ICESat-2 ATL03 data by application of the DDA-bifurcate, described in section (3.5). To demonstrate the DDA-bifurcate capabilities, we apply the algorithm to examples from two different environments: (1) The Amery Ice Shelf in East Antarctica, where large melt streams formed during a melt event in January 2019 (Fig. 2a) (Fricker et al., 2020) and (2) the region of the drainage basin of Sermeq Kujaleq (Jakobshavn Isbræ, Ilulissat Ice Stream), West Greenland. The Greenland region provides examples during of several stages of melt pond formation.

[FIGURE 2 here]

### 5.1 Large Melt Streams Amery Ice Shelf

The Amery Ice Shelf encompasses a small portion of the Antarctic coastline, but drains water from 16% of the total mass of the East Antarctic Ice Sheet (Fricker et al., 2002). In this work, four melt ponds from the Amery Ice shelf are examined (Fig. 2b-e), which were recorded in ICESat-2 RGT 81, beam gt2l (strong, green in Fig. 2a), on January 2, 2019 and in same-day Landsat-8 data (Fricker et al., 2020). We analyze the same examples here.

The morphology of the melt streams varies across the four examples. Figure 2b exemplifies two adjacent melt streams of approximately 5 m depth, which perhaps were part of a larger connected melt stream system that was divided by a frozen center. The melt streams have a diameter of several hundred meters (800 m for both streams combined). Figure 2c depicts a melt stream with a variable and rough ice bottom, which could indicate refreezing at the base of the stream. The third example captures two separate melt streams, with the second stream located close to the edge of Amery Ice stream (Fig. 2e). The edge of the second pond (at 2.1258 $\times 10^6$ m along-track distance) continues seamlessly from the slope outside of the pond to the sub-pond area, which illustrates that the bifurcation algorithm and the ground follower work together resulting in morphologically realistic representations. This gives credibility to the variable shapes of other stream edges. Figure 2f depicts a single, large melt stream with a smooth bottom ice surface and a maximal depth of 8 m. Notably, the DDA-bifurcate avoids the saturation effect that can affect ICESat-2 data and is seen in the secondary horizontal high-density area at an apparent location of 0.43m below the surface (at 2.1258 $\times$ $10^6$ m along-track distance). Instead of defaulting to the secondary false signal (range delay), the DDA-bifurcate correctly identifies the pond bottom. The DDA-bifurcate algorithm detects all ponds/melt streams and does not report false positives (Fig. S3).

### 5.2 Melt Ponds on the Greenland Ice Sheet During Complex Formation Stages

The analysis of melt ponds in the Sermeq Kujalleq (Ilulissat Ice Stream or Jakobshavn Isbræ) drainage basin, Greenland, is used to demonstrate that the DDA-bifurcate can be used to provide information on the characteristics of melt pond formation, which is sufficiently detailed to form a data basis for analysis of glacio-hydrological processes. For four ponds in the Sermeq Kujalleq drainage basin, we compare cross-sections of surface heights from ICESat-2 data with Landsat-8 imagery (Fig. 2d,g-n, S3).

Figures 2g,i show a fully developed melt pond with a continuous pond bottom at approximately 4m depth seen in the DDA-bifurcate result and a deep-blue, continuous pond surface seen in the Landsat-8 image. With no ice or firn obstructing the surface, the DDA-ice-bif algorithm accurately identifies the the edges of the pond along with a very distinct bottom surface. Density of the pond surface is high, resultant from high reflectivity of the water surface, whereas the pond bottom has a low density and photons are returned from a region with a vertical spread, indicating penetration of the 532 nm signal into the pond bottom material.

Melt ponds during the formation process are detectable with the DDA-bifurcate (Fig. 2h,j,k,m) as well. At the initial stage of formation, an emerging melt pond can take on a crescent shape (Fig. 2h) with perimetral valleys of water that surround semi-solid ice (Example 2, Fig. 2j). As the melt process continues inwards from the perimeter, a medial ice island or floating ice structure can form, as depicted by the pond in Example 3 (Figs. 2k,m), which reaches depths of 8 m.

More complex melt scenarios can also be investigated with the DDA-bifurcate, as depicted in Example 4 (Figure 2l,n), where a pond forms in variable cryospheric surface types, ranging from near molten ice closer to the interior of the pond to solid, undisturbed ice on the outside of the pond. The DDA-bifurcate reveals well-defined sections of melt and frozen or semi-frozen ice. The bottom of the pond has a wavy morphology and reaches depths of 7m. In the melt footprint, depth of the pond bottom varies between the three individual melt areas detected and is non-uniform, which the DDA-bifurcate handles well. The melt process is likely the result of several melt and refreezing instances. Thus, the need for accurate detection of melt features is demonstrated by Fig. 2n because, as the melt process continues from relatively new melting occurrences, more complex morphologies arise.

An approach for melt-pond determination, described in (Arndt & Fricker, 2024) and applied to ponds on the Greenland Ice Sheet, is limited to analysis of features of a minimum along-track size of 140 m and relatively clear surface and bottom representation in the ATL03 photon point cloud. In contrast, the DDA-bifurcate does not require a-priori information on the location of water bodies; it is a fully automated algorithm for detection of water features across a large range of sizes and types of complexity, with determination of the heights of the top and bottom surfaces, wherever such exist, and defaults to the (single) ice-surface height between ponds.

## 6 Summary and Conclusions

### 6.1 Overview and Mathematical Methods

This paper describes an approach for detection and measurement of supraglacial and near-surface water in ICESat-2 ATLAS data, to provide information on two essential and characteristically different processes: glacial acceleration and melting. As water in crevasses can also be the indicator of changes in the englacial hydrological system of a glacier which are hard to observe directly, but provide key information on the surge process, we use the terminology of "water-in-ice" as the focus for the objectives of this paper.

The DDA family of algorithms, which include first-order (DDA-ice-1) (U. Herzfeld et al., 2017; U. Herzfeld, Trantow, et al., 2021) and second-order algorithms (DDA-ice-2 and DDA-bifurcate) (U. Herzfeld et al., 2023), facilitates an analysis of ICESat-2 ATL03 photon data sets that is suited to provide the basis for cryospheric process studies, as complex surface types are correctly identified and extracted from the photon point cloud. The main concepts and mathematical principles of the algorithms are described in this paper. Results of the DDA-ice-2 include signal-photon classification and first- and second-order surface height profiles of the ice surface and crevasse bottoms. Importantly, we find that distinction between different cryospheric materials such as snow, old snow/firn, water-logged firn and water in crevasses is possible based on signal photon density relative to background noise density in crevasses. Thus, the analysis in this paper also indicates that the density field holds characteristic information about the relationship between cryospheric materials and their interaction with the 532nm signal of the ATLAS system, which is a problem that has only been tapped into superficially (Smith et al., 2018).

The DDA-bifurcate facilitates automated detection of melt ponds and melt streams without a-priori information on location and returns surface heights of the ice surface and the melt-feature bottom (where recorded in the data), it defaults to the (single) ice-surface height between ponds. All DDA-ice algorithms are auto-adaptive w.r.t. changes in background typical of day-time and night-time data. As such, the DDA-bifurcate constitutes a significant advance over previous work on detection of melt features on land ice.

The only limitation to detection of water in ice, based on ICESat-2 data, is the along-track distribution of the coverage typical of satellite altimeter data, which suggests that image data be used in addition.

### 6.2 Geophysical Applications and Results

Geophysical applications center on two problems: (1) The surge process, and there, the detection of crevasses and of water and other types of cryospheric material inside them, exemplified for the current (2016-present, 2024) surge of the Negribreen Glacier System, Svalbard. (2) Melt processes, as manifested in the examples of large melt streams in the Amery Ice Shelf, Antarctica, and smaller ponds indicative of complex morphogenetic processes in the drainage basin of Sermeq Kujaleq, Greenland. Airborne validation data, collected in August 2019 during the Negribreen surge (U. C. Herzfeld et al., 2022), is used to demonstrate accuracy of results.

**Surging.** In the first set of case studies, we apply the DDA-ice-1 and the DDA-ice-2 to capture the two most significant stages of a surge: (1) The first stage of a surge is characterized by formation of fresh crevasses with typically clear-cut edge, which are the signature of the rapid acceleration that occurs as the surge starts. These are found by application of the DDA-ice-1.

(2) The occurrence of water-filled crevasses marks the start of the mature surge phase. The occurrence of water-filled crevasses is the signature of a transition from an EDS to an IDS, where established drainage pathways are destroyed and the water flow through the glacier system is altered (Kamb, 1987; Trantow & Herzfeld, 2024a). ICESat-2 data analysis with the DDA-ice-2 yields unique data on water in crevasses as a signature of otherwise hard-to-observe changes in the interior of the glacier. In conclusion, the new detection capability will enable us to investigate the processes that control the unique dynamics of a surge and the hitherto incompletely understood evolution of hydrological changes.

**Melting.** Case studies of melt features, analyzed using the DDA-bifurcate, demonstrate that the algorithm can provide valuable data sets for the study of melt evolution. In an analysis of ICESat-2 data collected during a rare melt event in the Amery Ice Shelf in East Antarctica in January 2019, the DDA-bifurcate was applied to detect large melt streams that extended across a significant portion of the Amery Ice Shelf. This is a relatively simple detection problem, as the melt stream crossings measured several hundred meters. Augmenting the melt part of our study, smaller and more complexly shaped melt ponds are observed in the Sermeq Kujaleq (Ilulissat Ice Stream) drainage basin of the Greenland Ice Sheet. Here, the DDA-bifurcate is applied to create data sets that document several stages of the melt-formation process, providing spatial and depth information from ICESat-2 data and Landsat-8 image data. Again, we can see that the DDA yields information that is not easily (or not at all) attainable otherwise.

## Open Research Section

(1) ICESat-2 data products, e.g. ATL03, are freely available through NASA at https://earthdata.nasa.gov/ (release 3 and 4 used in this paper) and is provided by the National Snow and Ice Data Center (NSIDC).

(2) Data collected as part of the Negribreen Airborne Geophysical Campaigns, collected by the authors and their extended team, are available through the NSF Arctic Data Center and can be accessed at https://arcticdata.io/data/10.18739/A2QF8JK7T (U. C. Herzfeld & Trantow, 2021).

(3) Landsat-8 data are freely available through the U.S. Geological Survey, e.g., through the USGS Global Visualization Viewer (GloVis) (https://glovis.usgs.gov/).

## Acknowledgments

Thanks are due to Matthew Lawson, Jacob Hans and Camden Opfer, all members of the Geomathematics, Remote Sensing and Cryospheric Sciences Laboratory at the University of Colorado Boulder, for contributions to DDA-ice algorithm development and parameter optimization, to the ICESat-2 Project, especially Thomas Neumann, Nathan Kurtz, David Hancock and Anthony Martino for collaboration and support regarding ICESat-2. Maxar WorldView value-added image data products were received through the Polar Geospatial Center, University of Minnesota, Minnesota, U.S.A. Research and data collection were supported by the U.S. National Aeronautics and Space Administration (NASA) Earth Sciences Division under awards 80NSSC18K1439 and 80NSSC20K0975 by the U.S. National Science Foundation (NSF) under awards OPP-1745705 and OPP-1942356 (Office of Polar Programs); Principal Investigator for all awards is Ute Herzfeld. The helicopter was provided by the Norwegian Polar Institute and operated by Airlift. Collection of airborne data was conducted with permission of the National Security Authority of Norway, the Civil Aviation Authority of Norway and the Governor of Svalbard, registered as Research in Svalbard Project RIS-10827 "NEGRIBREEN SURGE". The data collection was also partly supported through a 2018 Access Pilot Project (2017_0010) of the Svalbard Integrated Observing System (SIOS). All this support is gratefully acknowledged. All this support is gratefully acknowledged.

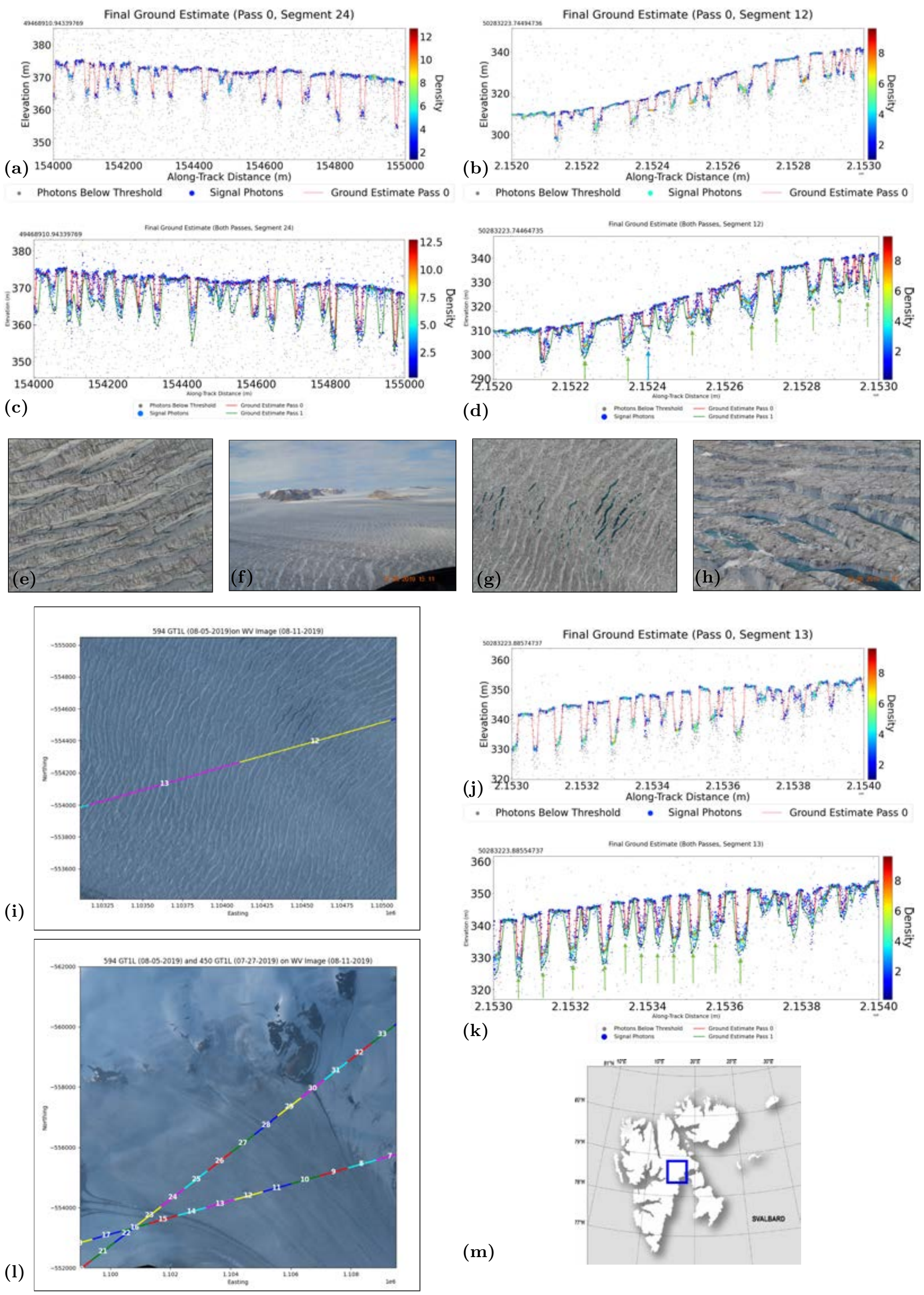


**Figure 1. Detection of dry crevasses and water in crevasses on Negribreen Glacier System, during the maturing phase of its surge (2019).** *Caption continued on next page.*

**Figure 1. Detection of dry crevasses and water in crevasses on Negribreen Glacier System, during the maturing phase of its surge (2019).** Comparison of analyses with the DDA-ice-1, DDA-ice-2, airborne image data collected during the 2019 ICESat-2 airborne validation campaign, and WorldView imagery. (a, b, j) Primary surface detected in ICESat-2 ATL03 data over surge crevasses on upper Negribreen during the surge, using the DDA-ice-1. Ground follower and density field from density-run 1, with signal photons identified by large dots with dot color indicating density. (a) DDA-ice-1 photon classification, density field and ground follower from ICESat-2 ATL03 data from RGT 450-1L, collected 2019-07-25, strong beam, day-time data, granule ATL03_20190727132129_04500405_004_01_gt1l, segment 24 (for relationship between beams and spots, see Fig. 3 and Table 1 in (U. C. Herzfeld et al., 2022));(b) DDA-ice-1 photon classification, density field and ground follower from ICESat-2 ATL03 data from RGT594-1L, collected 2019-08-05 at dusk, strong beam, granule ATL03_20190805232841_05940403_004_01_gt1l, segment 12(c) DDA-ice-2 photon classification, density field and ground follower from ICESat-2 ATL03 data from RGT 450-1L, collected 2019-07-25, day-time data, granule ATL03_20190727132129_04500405_004_01_gt1l, segment 24, matching DDA-ice-1 run in Fig. 1a;(d) DDA-ice-2 photon classification, density field and ground follower from ICESat-2 ATL03 data from RGT594-1L, collected 2019-08-05 at dusk, strong beam, granule ATL03_20190805232841_05940403_004_01_gt1l, segment 12, matching DDA-ice-1 run in Fig. 1b. Green arrows indicate water-logged firn, blue arrow standing water in crevasses.(e - h) Photographs of ice surface, taken during ICESat-2 airborne validation campaign, 2019-August-13. Locations of images matched to ICESat-2 ATL03 data using GPS data from airborne campaign (Fig. S2) (U. C. Herzfeld & Trantow, 2021). Strong beam and corresponding weak beam do not map the same ground locations due to 90-m ground track separation and along-track separation.(e) GoPro for RGT 450.1L (collapsed snow bridges),(f) Photo for RGT 450.1L,(g) GoPro for RGT 594.1L (water in crevasses),(h) Photo for RGT 594.1L. (i) Ground-track location of ICESat-2 ATL03 data from RGT594 GT1L: Fig. 1b,d segment 12 crevasses filled with water and water-logged firn , Fig. 1j,k segment 13 crevasses with water-logged firn, superimposed on WorldView 2 multispectral image from 2019-August-11 (WV02_20200801124218_10300100AA721300_20AUG01124218-M1BS-504570334070_01_P004_u16ns3413.tif),(j) DDA-ice-1 photon classification, density field and ground follower from ICESat-2 ATL03 data from RGT594-1L, collected 2019-08-05 at dusk, strong beam, granule ATL03_20190805232841_05940403_004_01_gt1l, segment 13 (k) DDA-ice-2 photon classification, density field and ground follower from ICESat-2 ATL03 data from RGT594-1L, collected 2019-08-05 at dusk, strong beam, granule ATL03_20190805232841_05940403_004_01_gt1l, segment 13, matching DDA-ice-1 run in Fig. 1j. Green arrows indicate water-logged firn in crevasses.(l) Ground-track location of ICESat-2 ATL03 data from RGT450 GT1L and RGT450 GT1L superimposed on WorldView 2 multispectral image from 2019-August-11 (same image as in Fig. 1i).(m) Location of Negribreen Glacier System in Svalbard.

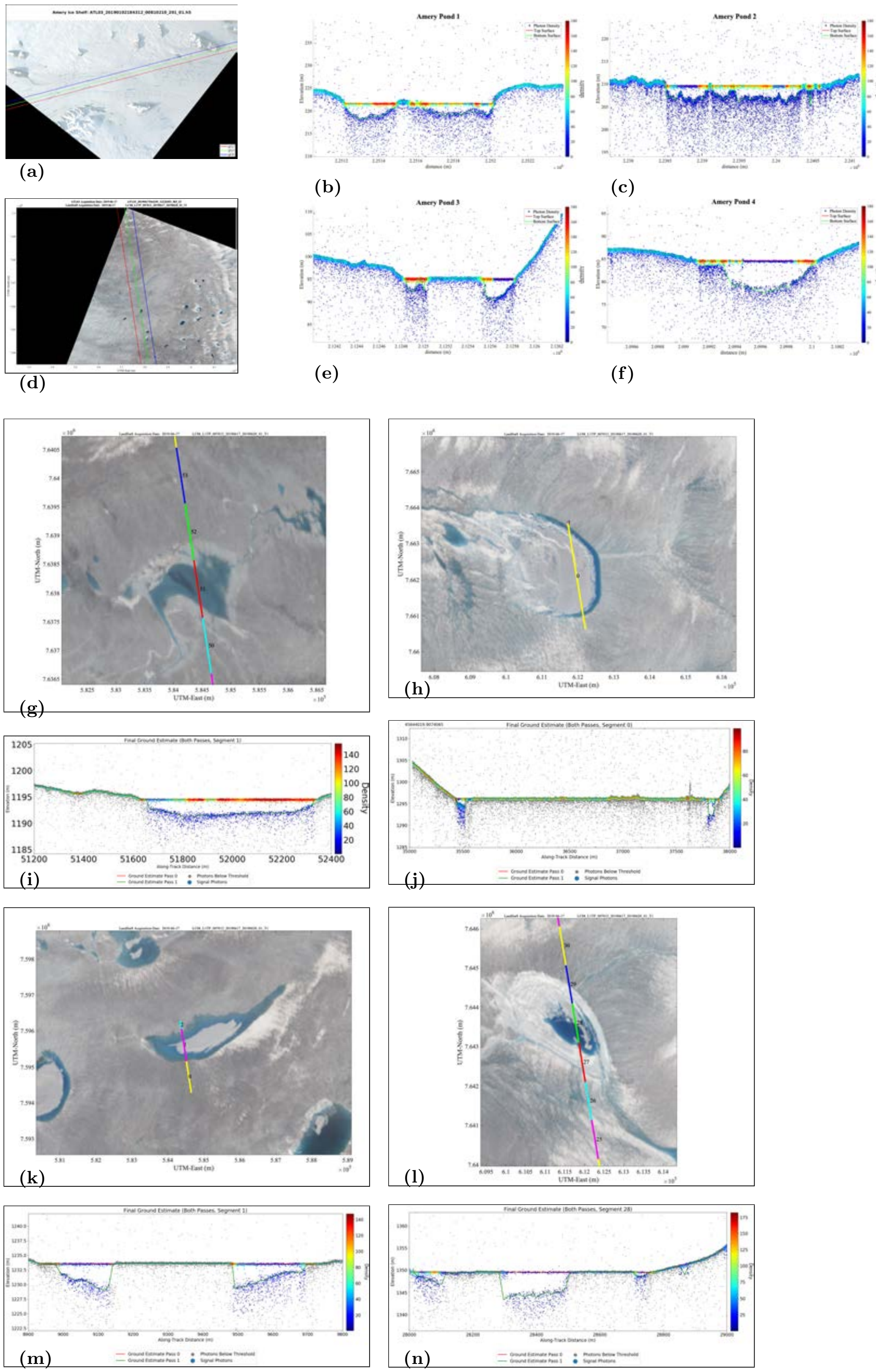


**Figure 2. Identification of melt ponds and measurement of pond depth.** *Caption continued on next page.*

**Figure 2. Identification of melt ponds and measurement of pond depth.** (a) Ground-track location of ICESat-2 ATL03 data from 2019-01-02, RGT81, Granule ATL03_20190102184312_00810210_003_01.h5, with center beam 81-2L in green, the beam used for analysis in (Fig. 2b,c,e,f) and Figure S1. Plotted over same-day Landsat-8 imagery (Jan 2, 2019). (b,c,e,f) Analysis of melt streams on Amery Ice Shelf with DDA-bifurcate for the ATL03 RGT beam in (a). Note pond depth is pseudo-depth (not corrected for speed of light in meltwater).(d) Overview of ICESat-2 tracks for RGT-1161 on Jakobshavn drainage basin over Landsat image from 2019-06-17. (g)-(n) Melt ponds in Sermeq Kujalleq (Ilulissat Ice Stream/ Jakobshavn Isbræ) drainage basin, Greenland, from ICESat-2 ATLAS data from 2019-06-17 [RGT 1222] (g,i) and 2019-06-13 [RGT 1161] (k, m) with corresponding Landsat imagery, collected 2019-06-17 (f,h,j,l), same-day for RGT 1222 and 4-days apart for RGT 1161. (g,i) Simple melt pond with clear water surface [from ICESat-2 granule ATL03_20190617064249_12220303_003_ 01.h5 channel gt1l](h, j) Melt pond during formation [from ICESat-2 granule ATL03_20190617064249_12220303_003_01.h5 channel gt1l] Landsat8 image from 2019-06-17. Same day as ICESat-2 data set.(k,m) Complex situation of floating ice, developing melt pond and frozen ice areas.Landsat8 image from 2019-06-17. ICESat-2 data collected 2019-06-13, just 4 days before the Landsat-8 image. [ATL03_20190613065109_11610303_ 003_ 01.h5, RGT 1161, channel gt2l].(l,n) Melting starting around the edges of a future pond. Landsat8 image from 2019-06-17. ICESat-2 data collected 2019-06-13, just 4 days before the Landsat-8 image. [ATL03_20190613065109_11610303_ 003_ 01.h5 RGT 1161, RGT 1161, channel gt3l.]

## References

Arndt, P. S., & Fricker, H. A. (2024). A framework for automated supraglacial lake detection and depth retrieval in icesat-2 photon data across the greenland and antarctic ice sheets. *The Cryosphere*, *18*(11), 5173–5206. doi: 10.5194/tc-18-5173-2024

Banerjee, D., Garg, V., & Thakur, P. K. (2022). Geospatial investigation on transitional (quiescence to surge initiation) phase dynamics of Monacobreen tidewater glacier, Svalbard. *Advances in Space Research*, *69*(4), 1813–1839.

Bartholomew, I., Nienow, P., Sole, A., Mair, D., Cowton, T., & King, M. A. (2012). Short-term variability in greenland ice sheet motion forced by time-varying meltwater drainage: Implications for the relationship between subglacial drainage system behavior and ice velocity. *Journal of Geophysical Research: Earth Surface*, *117*(F3).

Buckley, E. M., Farrell, S. L., Herzfeld, U. C., Trantow, T. M., Baney, O. N., Duncan, K., … Webster, M. (2023). Observing the evolution of summer melt on multiyear sea ice with ICESat-2 and Sentinel-2. *The Cryosphere*, *17*(9), 3695-3719. (Published 2023/08/31) doi: 10.5194/tc-17-3695-2023

Clarke, G. (1987). Fast glacier flow: Ice streams, surging, and tidewater glaciers. *Journal of Geophysical Research*, *92*, 8835–8842.

Farrell, S., Duncan, K., Buckley, E., Richter-Menge, J., & Li, R. (2020). Mapping sea ice surface topography in high fidelity with ICESat-2. *Geophysical Research Letters*, *47*(21), e2020GL090708. doi: 10.1029/2020GL090708

Fricker, H. A., Allison, I., Craven, M., Hyland, G., Ruddell, A., Young, N., … Popov, S. (2002). Redefinition of the amery ice shelf, east antarctica, grounding zone. *Journal of Geophysical Research: Solid Earth*, *107*(B5), ECV 1-1-ECV 1-9. Retrieved from `https://agupubs.onlinelibrary.wiley.com/doi/abs/10.1029/2001JB000383` doi: https://doi.org/10.1029/2001JB000383

Fricker, H. A., Arndt, P., Brunt, K., Tri Datta, R., Fair, Z., Jasinski, M., … Wouters, B. (2020). ICESat-2 Meltwater Depth Estimates: Application to Surface Melt on Amery Ice Shelf, East Antarctica. *Geophysical Research Letters*, *48*. doi: 10.1029/2020GL090550

Hall, D. K., Comiso, J. C., DiGirolamo, N. E., Shuman, C. A., Box, J. E., & Koenig, L. S. (2013). Variability in the surface temperature and melt extent of the greenland ice sheet from modis. *Geophysical Research Letters*, *40*(10), 2114–2120.

Herzfeld, U., Hayes, A., Palm, S., Hancock, D., Vaughan, M., & Barbieri, K. (2021). Detection and Height Measurement of Tenuous Clouds and Blowing Snow in ICESat-2 ATLAS Data. *Geophysical Research Letters*, *48*. doi: 10.1029/2021GL093473

Herzfeld, U., McDonald, B., & Weltman, A. (2013). Bering Glacier and Bagley Ice Valley surge 2011: Crevasse classification as an approach to map deformation stages and surge progression. *Annals of Glaciology*, *54(63)*, 279–286. doi: 10/3189/2013AoG63A338

Herzfeld, U., Palm, S., Hancock, D., Hayes, A., & Barbieri, K. (2022). *ICESat-2 Algorithm Theoretical Basis Document for the Atmosphere, Part II: Detection of Atmospheric Layers and Surface Using a Density Dimension Algorithm, v14.0, August 30, 2022, Geomath Code Version v120.0, ASAS Code Release v5.6, ATLAS Data Product ATL09.* NASA ICESat-2 Project. (477p) doi: 10.5067/CP08GNGYS4YJ

Herzfeld, U., Trantow, T., Buckley, E., Farrell, S., & Lawson, M. (2023). Automated detection and depth measurement of melt ponds on sea ice from ICESat-2 ATLAS data — the DDA-bifurcate-seaice. *IEEE Transactions of Geoscience and Remote Sensing*, 1-16. (published April 18, 2023) doi: 10.1109/TGRS.2023.326807

Herzfeld, U., Trantow, T., Harding, D., & Dabney, P. (2017). Surface-height determination of crevassed glaciers — Mathematical principles of an Auto-Adaptive Density-Dimension Algorithm and validation using ICESat-2 Simulator (SIMPL) data. *IEEE Transactions in Geoscience and Remote Sensing*, *55*(4), 1874–1896. doi: 10.1109/TGRS.2016.2617323

Herzfeld, U., Trantow, T., Lawson, M., Hans, J., & Medley, G. (2021). Surface heights and crevasse types of surging and fast-moving glaciers from ICESat-2 laser altimeter data — Application of the density-dimension algorithm (DDA-ice) and validation using airborne altimeter and Planet SkySat data. *Science of Remote Sensing*, *3*, 1-20. doi: 10.1016/j.srs.2020.100013

Herzfeld, U. C., Lawson, M., Trantow, T., & Nylen, T. (2022). Airborne Validation of ICESat-2 ATLAS Data Over Crevassed Surfaces and Other Complex Glacial

Environments: Results From Experiments of Laser Altimeter and Kinematic GPS Data Collection From a Helicopter Over a Surging Arctic Glacier (Negribreen, Svalbard). *Remote Sensing*, *14*, 1185-1224. doi: 10.3390/rs14051185

Herzfeld, U. C., & Trantow, T. (2021). *Airborne Laser Altimeter, Global Positioning System (GPS), Inertial Measurement Unit (IMU) and Imagery Campaign of the Surging Negribreen Glacier, Svalbard, in July 2017 and July 2018.* `https://arcticdata.io/catalog/view/doi:10.18739/A23J39249`. doi: 10.18739/A23J39249

Kamb, W. B. (1987). Glacier Surge Mechanism Based on Linked Cavity Configuration of the Basal Water Conduit System. *Journal Geophys. Res.*, *92*(B9), 9083-9100.

Kochtitzky, W., Winski, D., McConnell, E., Kreutz, K., Campbell, S., Enderlin, E. M., ... Jiskoot, H. (2020). Climate and surging of Donjek glacier, Yukon, Canada. *Arctic, Antarctic, and Alpine Research*, *52*(1), 264–280.

Liu, J., Enderlin, E. M., Bartholomaus, T. C., Terleth, Y., Mikesell, T. D., & Beaud, F. (2024). Propagating speedups during quiescence escalate to the 2020–2021 surge of Sít'Kusá, southeast Alaska. *Journal of Glaciology*, 1–12.

Main, B., Copland, L., Flowers, G., Dow, C., Van Wychen, W., Samsonov, S., & Kochtitzky, W. (2024). Topographic and hydrological controls on partial and full surges of Little Kluane Glacier, Yukon. *Journal of Glaciology*, 1–37.

Markus, T., Neumann, T., Martino, A., Abdalati, W., Brunt, K., Csatho, B., ... Zwally, J. (2017). The Ice, Cloud, and land Elevation Satellite-2 (ICESat-2): Science requirements, concept, and implementation. *Remote Sensing of Environment*, *190*, 260–273. doi: 10.1016/j.rse.2016.12.029

Markus, T., Stroeve, J., & Miller, J. (2009). Recent changes in arctic sea ice melt onset, freezeup, and melt season length. *Journal of Geophysical Research*, *114*(C12024), 1-14. doi: 10.1029/2009JC005436

Masson-Delmotte, V., Zhai, A., Pirani, S., Connors, C., Péan, S., Berger, N., ... Zhou, B. e. (2021). *AR6: Climate Change 2021: The Physical Science Basis. Contribution of Working Group I to the Sixth Assessment Report of the Intergovernmental Panel on Climate Change.* Cambridge University Press. doi: doi:10.1017/9781009157896

Mayer, H., & Herzfeld, U. (2000). Structural glaciology of the fast-moving Jakobshavn Isbræ, Greenland, compared to the surging Bering Glacier, Alaska, USA. *Annals of Glaciology*, *30*(1), 243–249.

McMillan, M., Nienow, P., Shepherd, A., Benham, T., & Sole, A. (2007). Seasonal evolution of supra-glacial lakes on the Greenland Ice Sheet. *Earth and Planetary Science Letters*, *262*(3-4), 484–492.

Moussavi, M. S., Abdalati, W., Pope, A., Scambos, T., Tedesco, M., MacFerrin, M., & Grigsby, S. (2016). Derivation and validation of supraglacial lake volumes on the Greenland Ice Sheet from high-resolution satellite imagery. *Remote sensing of environment*, *183*, 294–303.

Neumann, T., Brenner, A., Hancock, D., Robbins, J., Gibbons, A., Lee, J., ... Rebold, T. (2022a). *ATLAS/ICESat-2 L2A Global Geolocated Photon Data, Version 6.* NASA National Snow and Ice Data Center Distributed Active Archive Center. (Boulder, Colorado USA) doi: 10.5067/ATLAS/ATL03.006

Neumann, T., Brenner, A., Hancock, D., Robbins, J., Gibbons, A., Lee, J., ... Rebold, T. (2022b). *ICESat-2 Algorithm Theoretical Basis Document for Global Geolocated Photons ATL03, release 006, 2022.* NASA ICESat-2 Project. (211p) doi: 10.5067/GA5KCLJT7LOT

Neumann, T. A., Martino, A. J., Markus, T., Bae, S., Bock, M. R., Brenner, A. C., ... Thomas, T. C. (2019). The Ice, Cloud, and Land Elevation Satellite–2 mission: A global geolocated photon product derived from the Advanced Topographic Laser Altimeter System. *Remote Sensing of Environment*, *233*, 111325. doi: 10.1016/j.rse.2019.111325

Nghiem, S., Hall, D., Mote, T., Tedesco, M., Albert, M., Keegan, K., ... Neumann, G. (2012). The extreme melt across the greenland ice sheet in 2012. *Geophysical Research Letters*, *39*(20).

Oltmanns, M., Straneo, F., & Tedesco, M. (2019). Increased Greenland melt triggered by large-scale, year-round cyclonic moisture intrusions. *The Cryosphere*, *13*(3), 815–825.

Ryan, J., Smith, L., Van As, D., Cooley, S., Cooper, M., Pitcher, L., & Hubbard, A. (2019). Greenland Ice Sheet surface melt amplified by snowline migration and bare ice exposure. *Science Advances*, *5*(3), eaav3738.

Schoof, C. (2010). Ice-sheet acceleration driven by melt supply variability. *Nature*, *368*, 803–806.

Smith, B. E., Gardner, A., Schneider, A., & Flanner, M. (2018). Modeling biases in laser-altimetry measurements caused by scattering of green light in snow. *Remote Sensing of Environment*, *215*, 398–410.

Sneed, W., & Hamilton, G. S. (2007). Evolution of melt pond volume on the surface of the Greenland Ice Sheet. *Geophysical research letters*, *34*(3).

Spergel, J. J., Kingslake, J., Creyts, T., van Wessem, M., & Fricker, H. A. (2021). Surface meltwater drainage and ponding on amery ice shelf, east antarctica, 1973–2019. *Journal of Glaciology*, *67*(266), 985–998.

Stocker, T. F., Qin, H., Plattner, G.-K., Tignor, M., Allen, S. K., Boschung, J., ... Midgley, P. M. e. (2013). *Climate Change 2013: The Physical Science Basis. Contribution of Working Group I to the Fifth Assessment Report of the Intergovernmental Panel on Climate Change.* Cambridge University Press.

Stroeve, J. C., Mioduszewski, J. R., Rennermalm, A., Boisvert, L. N., Tedesco, M., & Robinson, D. (2017). Investigating the local-scale influence of sea ice on Greenland surface melt. *Cryosphere*, *11*(5), 2363–2381.

Sundal, A., Shepherd, A., Nienow, P., Hanna, E., Palmer, S., & Huybrechts, P. (2009). Evolution of supra-glacial lakes across the Greenland Ice Sheet. *Remote Sensing of Environment*, *113*(10), 2164–2171.

Tedesco, M., Mote, T., Fettweis, X., Hanna, E., Jeyaratnam, J., Booth, J., ... Briggs, K. (2016). Arctic cut-off high drives the poleward shift of a new Greenland melting record. *Nature Communications*, *7*(1), 1–6.

Trantow, T., & Herzfeld, U. C. (2018). Crevasses as indicators of surge dynamics in the Bering Bagley Glacier System, Alaska: Numerical experiments and comparison to image data analysis. *Journal of Geophysical Research: Earth Surface*, *123*(8), 1615–1637. doi: 10.1029/2017JF004341

Trantow, T., & Herzfeld, U. C. (2024a). Evolution of a Surge Cycle of the Bering-Bagley Glacier System From Observations and Numerical Modeling. *Journal of Geophysical Research: Earth Surface*, *129*(1), e2023JF007306. doi: 10.1029/2023JF007306

Trantow, T., & Herzfeld, U. C. (2024b). Progression of the surge in the Negribreen Glacier System from two years of ICESat-2 measurements. *Journal of Glaciology (accepted for publication 20-Jun-2024), Earth ArXiv (preprint: doi.org/10.31223/X5NT1Z)*. doi: doi.org/10.31223/X5NT1Z

Truffer, M., & Echelmeyer, K. A. (2003). Of isbrae and ice streams. *Annals of Glaciology*, *36*(1), 66–72.

Williamson, A., Banwell, A., Willis, I., & Arnold, N. (2018). Dual-satellite (sentinel-2 and landsat 8) remote sensing of supraglacial lakes in greenland.

Wood, M., Rignot, E., Fenty, I., Menemenlis, D., Millan, R., Morlighem, M., … Seroussi, H. (2018). Ocean-induced melt triggers glacier retreat in Northwest Greenland. *Geophysical Research Letters*, *45*(16), 8334–8342.

Zwally, H. J., Abdalati, W., Herring, T., Larson, K., Saba, J., & Steffen, K. (2002). Surface melt-induced acceleration of Greenland ice-sheet flow. *Science*, *297*(5579), 218–222.